Angewandte Chemie

Supporting Information

Interplay of Atomic Interactions in the Intermetallic Semiconductor Be$_5$Pt

Alfred Amon, Eteri Svanidze, Alim Ormeci, Marcus König, Deepa Kasinathan, Daisuke Takegami, Yurii Prots, Yen-Fa Liao, Ku-Ding Tsuei, Liu Hao Tjeng, Andreas Leithe-Jasper, and Yuri Grin*

anie_201909782_sm_miscellaneous_information.pdf

Materials and Methods

All sample preparation was performed in argon-filled glove boxes (MBraun, $p(H_2O/O_2)$ <0.1 ppm), dedicated to the handling of Be-containing samples [43]. The polycrystalline samples of Be_5Pt were prepared by arc melting of the elements Be (Heraeus, >99.9 wt%) and Pt (Chempur, >99.9 wt%). The material loss due to evaporation of Be was compensated by a small excess of it.

Powder X-ray diffraction was performed on a Huber G670 Image Plate Guinier Camera (Ge monochromator, Cu $K\alpha_1$ radiation, Fig. S1). Single-crystal X-ray diffraction data were recorded on a Rigaku AFC7 diffractometer equipped with a Saturn724+ CCD detector (Mo$K\alpha$ radiation) and analysed within the program package WinCSD [44].

Analysis of the microstructure of polycrystalline Be_5Pt samples showed that even in the samples of highest phase purity, large regions of single-phase Be_5Pt are interspersed with Be. The latter is hard to detect with the X-ray powder diffraction due to the low scattering power but dominates the bulk transport behaviour, making bulk samples appear metallic. With this in mind, we have fabricated a micro-scale device using Xe-plasma focused-ion-beam (FIB) patterning. A slice with dimensions of $150 \times 50 \times 2$ μm^3 was extracted from an arc-melted Be_5Pt sample and transferred to a SiO_2 substrate. In this slice, SEM analysis revealed two phases, as marked in Fig. 3: the main phase is Be_5Pt (gray) and the secondary one is Be (black). Due to the small thickness of the slice, both phase boundaries and imperfections are visible from either side, thus making it possible to identify regions, which consist only of Be_5Pt.

Temperature-dependent resistivity was measured in magnetic fields of $H = 0$ T and $H = 9$T. The measurements of the micro-scale device were performed using a standard four-point technique in a ^{4}He PPMS system, for temperatures between 2 K and 400 K. Polished surface of an arc-melted Be_5Pt sample was analysed using EDXS. The micro-scale device was fabricated in a multi-step process using Xe-plasma focused-ion-beam patterning. Details of these processes are similar to what has previously been done for other strongly correlated systems – for example, see Refs. [45-47] and references therein. This approach allows to investigate intrinsic electrical properties of a material such as Be_5Pt, for which both single-phase and single crystal manufacturing still remain challenging.

Hard X-ray photoelectron spectroscopy (HAXPES) experiments were performed at the Max-Planck-NSRRC HAXPES station at the Taiwan undulator beamline BL12XU at SPring-8 (Japan). Photoelectron spectra were recorded with an incident radiation of $hv = 6669$ eV and a MB Scientific A-1 HE photoelectron detector. The polycrystalline samples of Be_5Pt were cleaved in situ under ultrahigh vacuum conditions and the sample holder cooled to 80 K. After a wide scan ($E_{kin} = 3200\text{-}6675$ eV) to verify the purity of the investigated sample area, the core, semi-core and valence band spectra were recorded. No corrections beside subtraction of a constant background have been made to the data. Spectra of the valence band and Pt-$4f$ levels of Be_5Pt and Pt were recorded in parallel geometry (i.e. electron analyser in plane with the beam polarization plane). Spectra of Be-$1s$ levels were recorded in parallel and perpendicular (i.e. electron analyser normal to polarization plane) geometry. For s-orbitals a strong dependence of the photoionization cross section on the polarization direction of the incident beam relative to the electron detector is expected [48].

Electronic structure calculations were performed for Be_5Pt, Be_5Pd [49] and hypothetical Be_5Ni on the fully-, scalar- and non-relativistic level by using the all-electron, full-potential local orbital method (FPLO) [50] and Fritz-Haber-Institute ab-initio molecular simulations (FHI-aims [51]) packages. The local density approximation to the density functional theory as parameterised by Perdew-Wang [52] was employed to account for the exchange-correlation effects. The Brillouin zone was sampled with a mesh of $20\times20\times20$ k points. For comparison with the HAXPES valence band spectrum, the partial contributions to the calculated DOS of the valence band were weighted by their orbital-dependent photoionization cross sections [53] and a Gaussian broadening of 250 meV together with the Fermi-Dirac distribution function at $T = 100$ K was used.

The electron density and the electron localizability indicator in its ELI-D representation (Y_D) [34, 35, 54] were computed employing the interface implemented in the FHI-aims package [55].
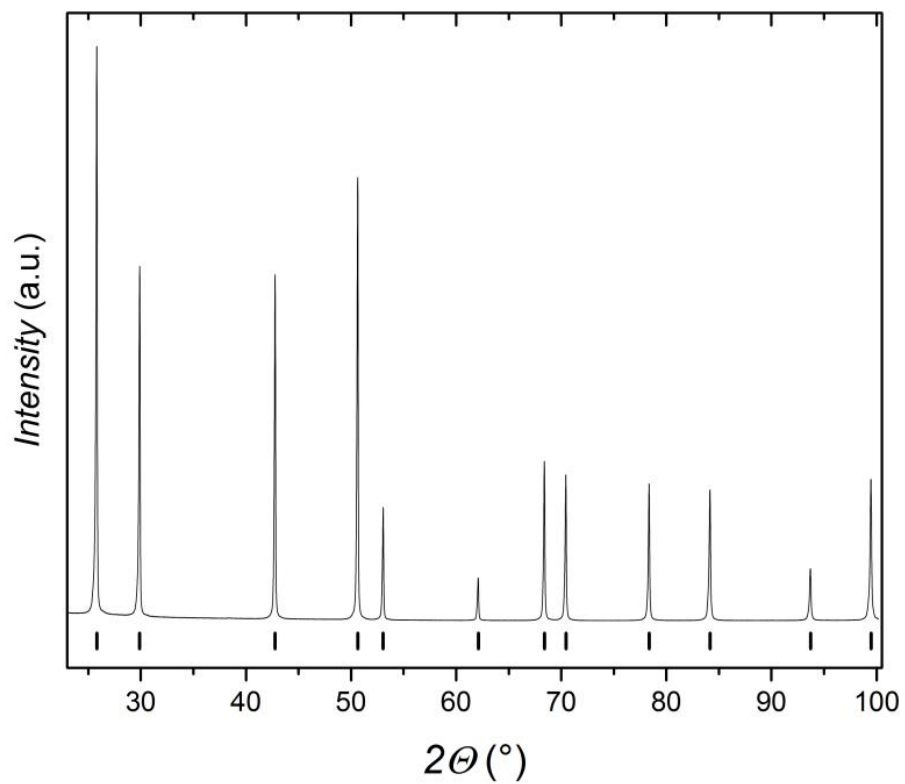
Figure S1.

X-ray powder diffraction pattern of Be_5Pt (CuK_{a1} radiation). The ticks show the reflection positions.
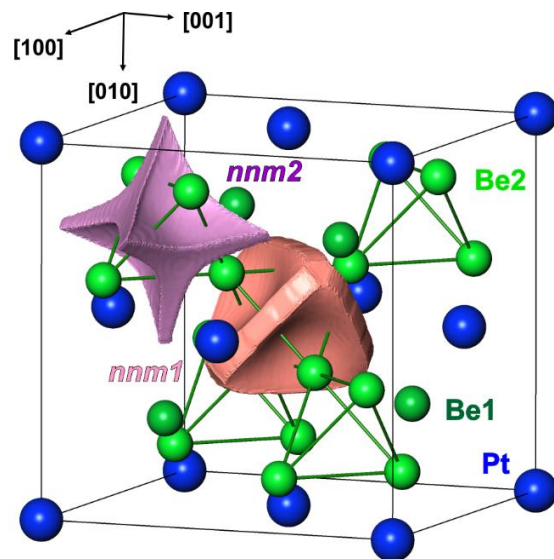
Figure S2.

The QTAIM basins of two types of non-nuclear maxima (light pink and light red) of the electron density in Be$_5$Pt (Pt – blue, Be1 –dark green, Be2 – light green). Both basins have the largest common surfaces (convex) with the atomic basins of Be2. Much smaller common surfaces with the atomic basins are flatter.
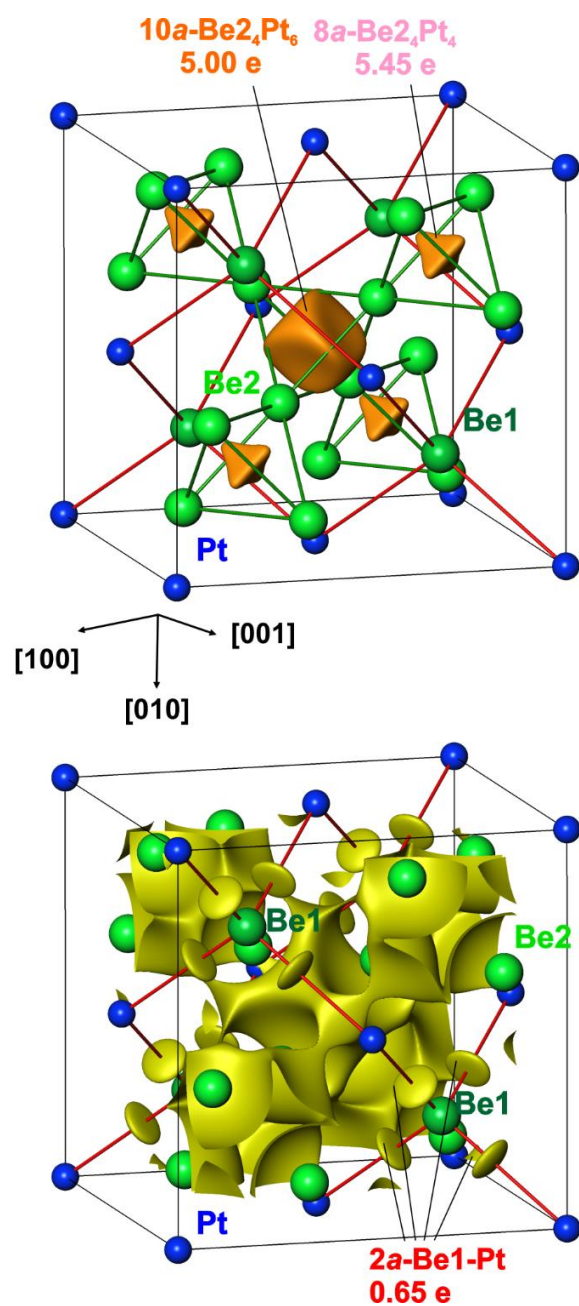
Figure S3.

Isosurfaces of ELI-D in Be_5Pt visualizing positions of the ELI-D maxima and populations of their basins: (upper panel) isosurface with ELI-D = 1.28 (orange) visualizes the 8*a*- and 10*a*-interactions within the tetrahedral network of Be2 atoms (green); (bottom panel) isosurface with ELI-D = 1.115 (greenish) visualizes the 2a-Be1-Pt bonds.
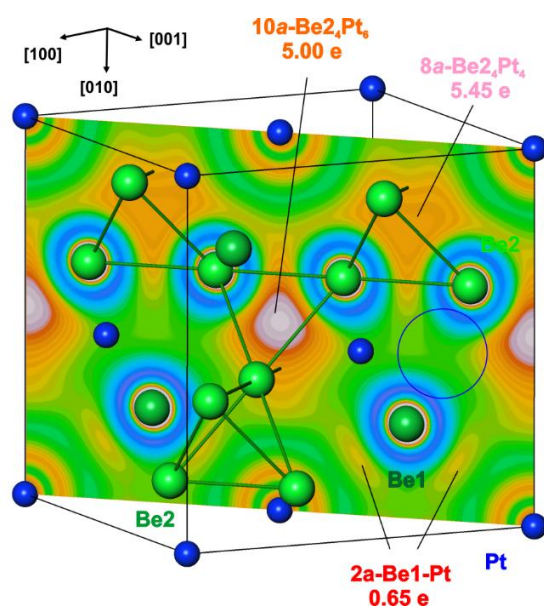
Figure S4.

ELI-D distribution in the (101) plane revealing no interaction between Be1 and Be2 atoms (blue circle).
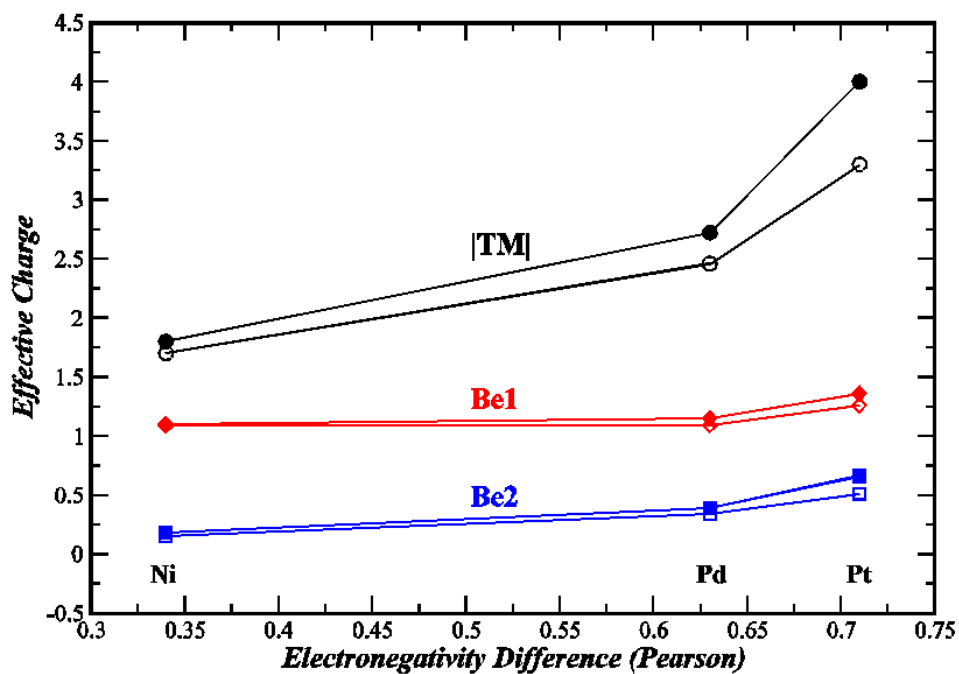
Figure S5.

Effective charges in Be$_5$*TM* compounds computed based on the QTAIM approach using both the nonrelativistic and scalar relativistic calculations. Full symbols are scalar relativistic, open ones nonrelativistic. Transition metal (*TM*) charges are negative, their absolute values are plotted. The lines are a guide for the eye. It is observed that in addition to the electronegativity difference, relativistic effects also contribute to charge transfer.
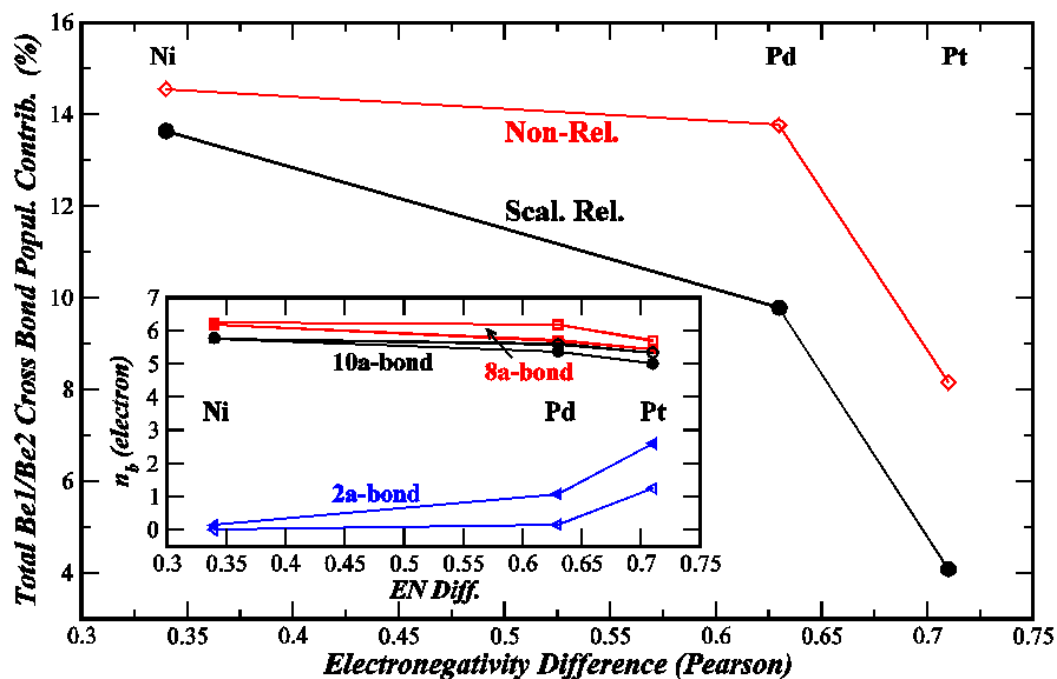
Figure S6.

Bonding in Be₅*TM* compounds: Be1 contributions to Be2-*TM*-based cluster bonds and Be2 contributions to two-atom Be1-*TM* bonds are quite small, and these contributions are referred to as cross contributions to the bond populations (n_b). Here, such cross contributions are expressed as a percentage of respective bond populations and the sum of these percentage values are plotted. The significantly small value in the relativistic calculation for Be₅Pt implies that covalent interactions between Be1 and Be2 atoms in this semiconducting compound are minimal. Inset: Populations of the three types of bonds are shown for each compound. For both figures, the lines are a guide for the eye, and full symbols are scalar relativistic, open ones nonrelativistic.
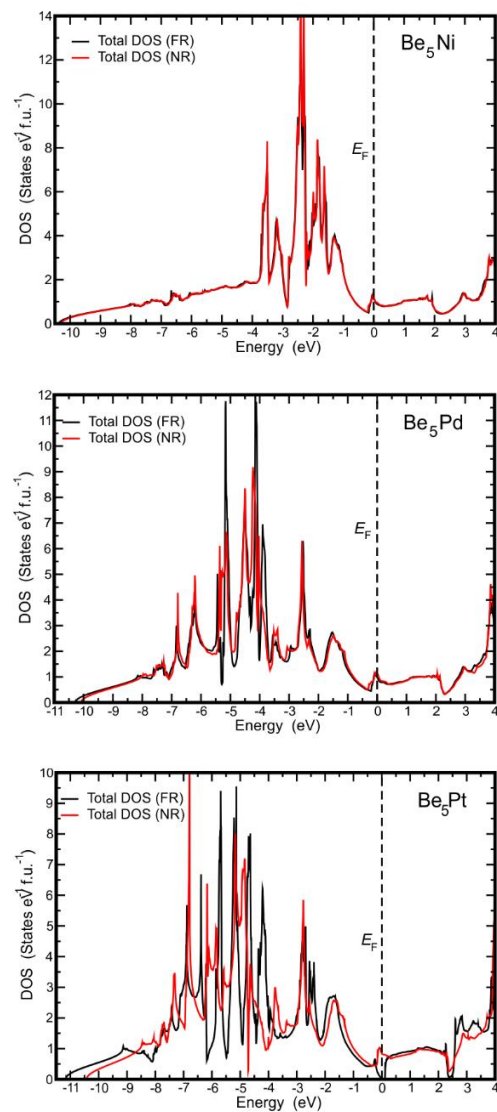
Figure S7

Calculated electronic DOS in fully relativistic (FR) and non-relativistic (NR) approximation for hypothetical Be₅Ni as well as existing Be₅Pd and Be₅Pt.
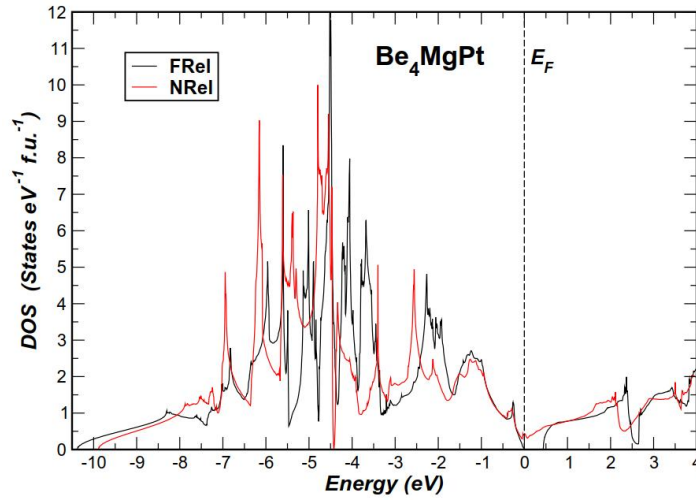
Figure S8 Calculated electronic DOS in fully relativistic (FRel) and non-relativistic (NRel) approximation for hypothetical Be_4MgPt.

The crystal structure was fully-optimized at the scalar relativistic level ($a = 6.1627$ Å, x(Be2) = 0.62576, force criterion was 1 meV Å-1). Electronic structure calculations were performed at non-, scalar- and fully relativistic levels using the optimized structure. Be_4MgPt turns out to be another example of a relativistic semiconductor. It has metallic DOS in a non-relativistic calculation, but at the scalar and fully relativistic levels it has a band gap of 0.44 eV. Just as in the case of Be_5Pt, spin-orbit interactions are not needed for opening up the gap, corrections at the scalar level are sufficient. In these FPLO calculations Be 2s and Mg 2s, 2p electrons were included in the valence (semi-core treatment). The DOS of Be_4MgPt and Be_5Pt (cf. bottom panel of Fig. S7) are highly similar implying that the valence electrons play the decisive role in these relativistic semiconductors.
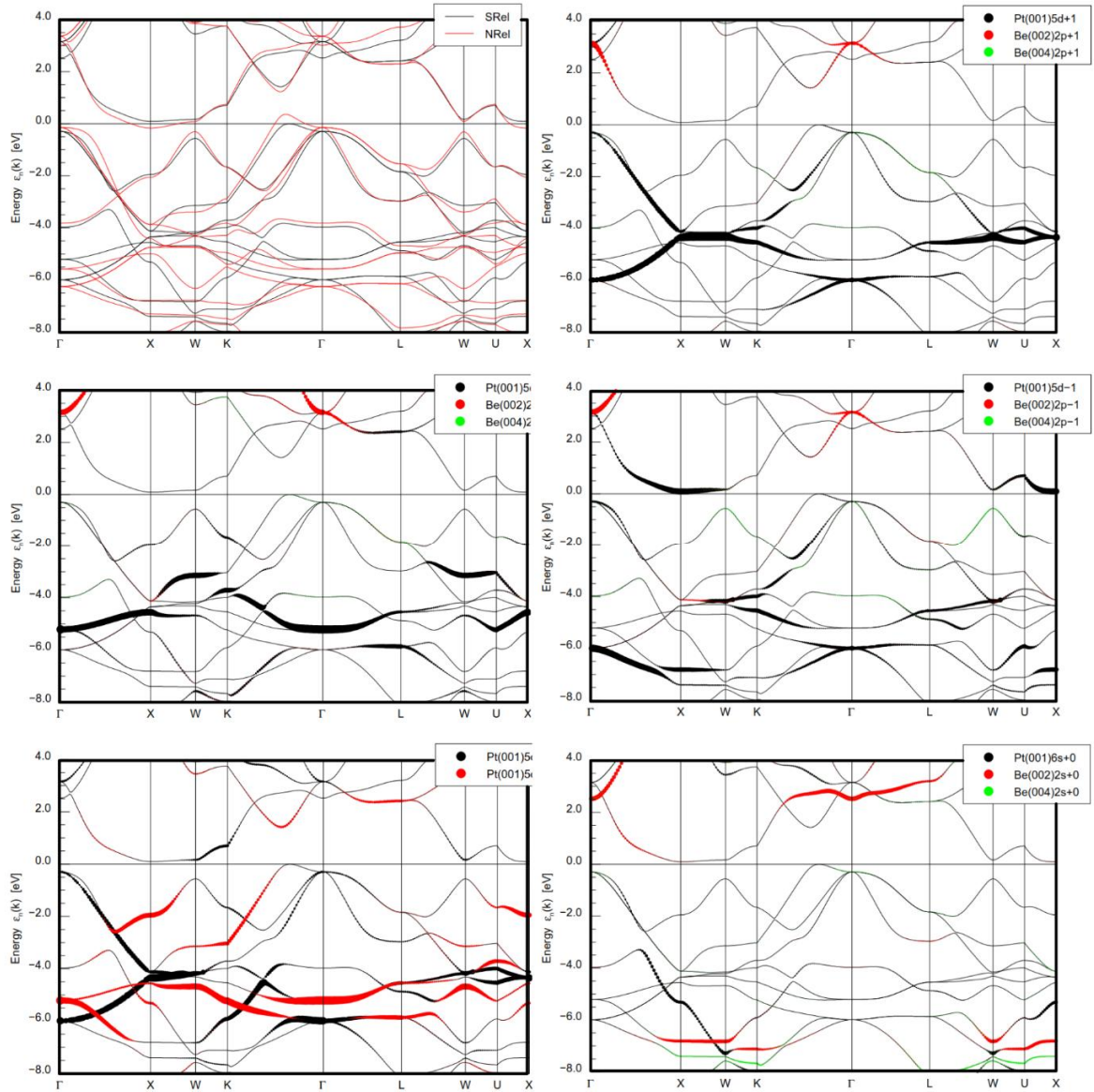
Figure S9. Calculated band structure of Be$_5$Pt: (top left panel) Comparison of the calculated band structure in scalar- (SRel) and non-relativistic (NRel) approximations; (other panels) Relative orbital contributions to the bands (fat-band plots); the size of the circle in the legends corresponds to 100% contribution.

 The top valence band (TVB) is triply (doubly) degenerate at Γ (along Γ – L), but at other points nondegenerate. The lowest-lying conduction band (LCB) is doubly degenerate around L and nondegenerate otherwise. The band gap observed at the scalar relativistic level is an indirect one: the highest occupied state is located between K and Γ, closer to the midpoint and the lowest unoccupied state is at X. The metallicity found at the nonrelativistic level is due to the former

11

state moving up and the latter one moving down in energy when the scalar relativistic corrections (relativistic energy-momentum relationship and Darwin shifts) are removed. The nature of this finding is highly similar to the one reported in the theoretical work on CsAu [90]. However, the electronic structure of Be_5Pt is definitely more complex than that of CsAu, because (*i*) Pt in Be_5Pt has a more complicated local environment (coordinated by 4 Be1 and 12 Be2) than that of Au in CsAu (coordinated by 8 Cs), and (*ii*) although the TVB and LCB of CsAu are formed by Au 6s and Cs 5d, Au 6p orbitals, respectively, the corresponding bands in Be_5Pt have the relevant parts of the contributions of varying amounts from 5d, 6s of Pt, and 2s, 2p of Be1 and Be2, cf. the fat-bands analysis. TVB of Be_5Pt have largest contributions as per atom from Pt 5d and Be2 2s, 2p orbitals. Be1 states have minimal contribution to TVB. Pt 5d contributions to the LCB are also significant (especially $5d_{zy}$ and $5d_{xy}$ at lower edge, $5d_{z2}$ and $5d_{x2-y2}$ at upper edge), and Be1 contributes to LCB more strongly than Be2 does (again one per atom basis). Consequently, it is not as clear cut as it is in the case of CsAu to determine how the scalar relativistic corrections will shift the TVB and LCB [90]. Nevertheless, the following observations can be made: (*i*) the section of the LCB responsible for metallization, i.e., the part moving below Fermi energy in the nonrelativistic treatment, is almost entirely made up from Pt $5d_{zy}$ orbital. Be1 2s and at somewhat lower levels 2p orbitals of both Be1 and Be2 also hybridize with Pt $5d_{zy}$; (*ii*) the section of the TVB responsible for metallicity, i.e., moving above the Fermi energy in the nonrelativistic treatment, has contributions from Pt $5d_{zy}$, $5d_{xy}$, and $5d_{x2-y2}$ orbitals as well as Be2 2s and 2p orbitals. In regard to the pseudo-gap at around 2.4 eV, the situation is similarly complicated. Some of the bands remain remarkably identical in both scalar and nonrelativistic treatments, although some others move up or down by varying amounts. The same avoided crossings are observed in both cases, but usually at slightly different energies and at different k-vectors. More importantly, the band width of the scalar relativistic LCB is smaller than that of the nonrelativistic LCB, and all these effects combine to round up the relatively sharp pseudo-gap of the scalar relativistic DOS.
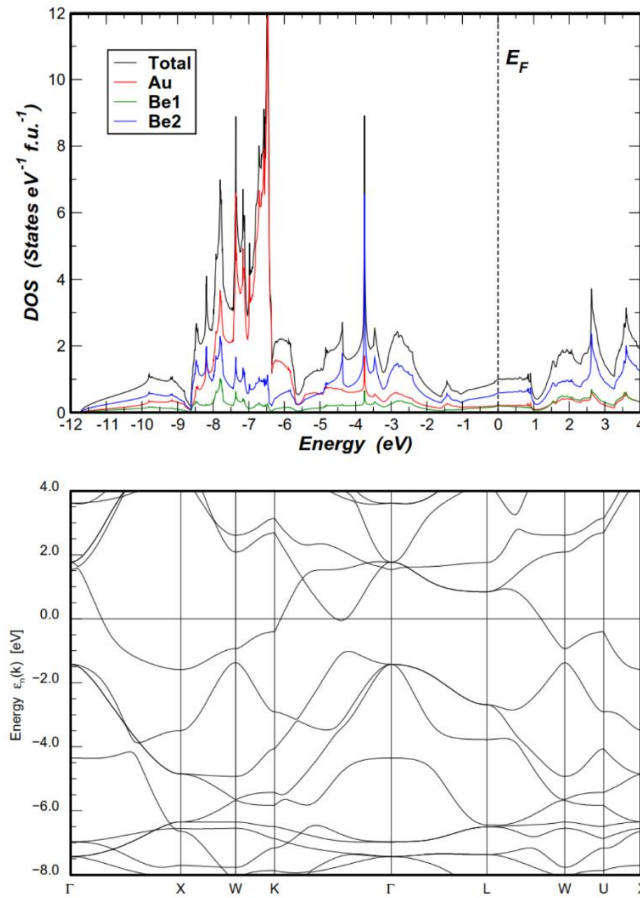
Figure S10. Scalar relativistic electronic structure of Be₅Au: (top) electronic DOS, (bottom) electronic band structure. Be₅Au has an odd number of electrons per primitive unit cell. Therefore, it is bound to be a metal. Electronic structure calculations on Be₅Au yield a metallic DOS at all relativistic levels (non, scalar and fully-relativistic). Comparison with the bands of Be₅Pt (Fig. S9) shows that the Fermi level in Be₅Au falls in the band corresponding to the lowest-lying conduction band of Be₅Pt. This band has approximately the same band width in both compounds (about 2.4 eV), and the metallicity of Be₅Au follows from the necessity of accommodating the extra electron of the Au atom in this band.

Table S1.
Examples of semiconducting materials

Composition	Structure type	E_g (eV)	Ref.
Si	Diamond	1.12	[56]
Ge	Diamond	0.66	[56]
GaAs	Sphalerite	1.42	[56]
CdTe	Sphalerite	1.49	[57]
ZnSe	Sphalerite	2.70	[58]
TiNiSn	MgAgAs	0.51	[59]
TiCoSb	MgAgAs	0.82	[60]
$SrSi_2$	$SrSi_2$	0.035	[61]
Ba_3Sn_2	Ba_3Sn_2	0.73	[62]
$BaSi_2$	$EuGe_2$	1.3	[63]
Ca_2Si	*anti*-$PbCl_2$	0.3	[64]
Ca_2Sn	*anti*-$PbCl_2$	0.12	[64]
Ca_2Pb	*anti*-$PbCl_2$	0.15	[64]
Ca_3AlSb_3	Ca_3InP_3	0.71	[65,65]
$CaMn_2Bi_2$	$CaAl_2Si_2$	0.06	[67]
$CaCd_2Sb_2$	$CaAl_2Si_2$	0.63	[68]
Mg_2Si	*anti*-CaF_2	0.4-0.8	[70]
Mg_2Ge	*anti*-CaF_2	0.69	[71,72]
Mg_2Sn	*anti*-CaF_2	0.22	[72]
HT-$MoSi_2$	$CrSi_2$	0.30	[73]
$CrSi_2$	$CrSi_2$	0.35	[74]
RuAl2	CrSi2	0.60	[75]
$RuGa_2$	$TiSi_2$	0.42	[76]
$OsAl_2$	$MoSi_2$	0.9	[77]
Ru_2Si_3	Ru_2Sn_3	0.7	[57]
Fe_2Ge_3	Ru_2Sn_3	0.03	[78]
ReGaSi	$MoSi_2$	0.2	[79]
$MnCoAl_4$	$TiSi_2$	0.51	[80]
$FeGa_3$	$IrIn_3$	0.3	[81,82]
$RuGa_3$	$IrIn_3$	0.3	[81,82]
$OsGa_3$	$IrIn_3$	0.42	[82]

ZnSb	CdSb	0.5	[83]
CdSb	CdSb	0.49	[84]
FeSi	FeSi	0.06	[85]
CsAu	CsCl	2.6-3.3	[86]
RbAu	CsCl	0.36	[87]
Cs$_2$Pt	Ni$_2$In	1.3-1.8	[88]

In this work we use the term 'intermetallic compounds' for the species formed by only elements located at and left of the Zintl line the Periodic Table [13]. This includes the compounds formed by triels and tetrels (normal font in Table S1) and such formed by the s- and d-metals which are called as made up exclusively by metallic elements (marked in the Table S1 in bold). The formulas of tetrahedral materials are given in italics.

Table S2.

Experimental details for single-crystal diffraction data on Be_5Pt

Diffraction system	Rigaku AFC7
Radiation; wavelength, λ	MoKα; 0.71073 Å
2θ max	85.9
N(hkl) measured	961
N(hkl) unique	61
N(hkl) observed (F(hkl) $> 4\sigma(F)$)	59
R_{int} / R_{σ}	0.0361 / 0.0130
Refined parameters	5
R_F / wR_F / goodness of fit	0.0103 / 0.0103 / 1.06
Weighting scheme	$w_i = [\ln(F^4_{obs,i})]^{-1}$
Residual electron density maxima	+0.34/-0.19 e Å^{-3}

Table S3.

Atomic coordinates and displacement parameters for Be_5Pt determined from single-crystal diffraction data

Atom	Site	x/a	y/b	z/c	B_{iso}/ Å²
Pt1	4a	0	0	0	0.454(7)
Be1	4c	¼	¼	¼	0.66(11)
Be2	16e	0.624(1)	x	x	1.2(3)

Table S4.

QTAIM charges (Q) and populations of bond basins with atomic contributions (in electrons) for Be$_5$TM compounds (TM = Pt, Pd, Ni (hypothetical)) as obtained from FHI-aims calculations in scalar-relativistic (SREL) and non-relativistic (NREL) approximations.

	Be$_5$Pt SREL	Be$_5$Pt NREL	Be$_5$Pd SREL	Be$_5$Pd NREL	'Be$_5$Ni' SREL	'Be5Ni' NREL
Q(*TM*)	-4.00	-3.30	-2.72	-2.46	-1.80	-1.70
Q(Be1)	+1.36	+1.26	+1.15	+1.09	+1.10	+1.09
Q(Be2)	+0.66	+0.51	+0.39	+0.34	+0.18	+0.15
Q(*nnm1*) at ½½½	-1.36	-1.40	-1.55	-1.58	-1.85	-1.86
Q(*nnm2*) at ¾¾¾	-0.75	-1.05	-1.08	-1.18	-1.61	-1.64
2*a*-*TM*Be1	0.65	0.31	0.27	0.04	0.033	does
TM	0.51	0.25	0.21	0.03	0.026	not
Be1	0.12	0.06	0.06	0.01	0.007	exist
6Be2	0.02	0.00	0.00	0.00	0.00	
10*a*-Be$_{24}$*TM*$_6$ at ½½½	5.00	5.34	5.37	5.59	5.77	5.77
nnm1	1.36	1.40	1.55	1.58	1.85	1.86
4Be2	1.44	1.69	1.68	1.76	1.72	1.75
6*TM*	2.12	2.04	1.86	1.87	1.76	1.70
4Be1	0.08	0.21	0.28	0.38	0.44	0.46
8*a*-Be$_{24}$*TM*$_4$ at ¾¾¾	5.45	5.70	5.70	6.18	6.17	6.24
nnm2	0.75	1.05	1.08	1.18	1.61	1.64
4Be2	1.46	1.69	1.80	1.91	1.83	1.87
4*TM*	3.24	2.72	2.56	2.66	2.36	2.32
6Be1	0.00	0.24	0.26	0.43	0.37	0.41

Additional references

44. A. Leithe-Jasper, H. Borrmann, and W. Hönle, In *Scientific Report of the Max-Planck-Institute for Chemical Physics of Solids 2003-2005* (MPI CPfS, Dresden, 2006), p. 24-27.

45. L. Akselrud, Yu. Grin, *J. Appl. Crystallogr. 47*, 803-805 (2014).

46. F. Ronning, T. Helm, K. R. Shirer, M. D. Bachmann, L. Balicas, M. K. Chan, B. J. Ramshaw, R. D. McDonald, F. F. Balakirev, M. Jaime, E. D. Bauer, P. J. W. Moll, *Nature*, *548*, 313-317 (2017).

47. M. D. Bachmann, N. Nair, F. Flicker, R. Ilan, T. Meng, N. J. Ghimire, E. D. Bauer, F. Ronning, J. G. Analytis, P. J. W. Moll, *Science Adv.*, *3*, 1602983 (2017).

48. P. J. W. Moll, *Ann. Rev. Cond. Mat. Phys. 9*, 147-162 (2018).

49. J. Weinen, T. C. Koethe, C. F. Chang, S. Agrestini, D. Kasinathan, Y. F. Liao, H. Fujiwara, C. Schüßler-Langeheine, F. Strigari, T. Haupricht, G. Panaccione, F. Offi, G. Monaco, S. Huotari, K.-D. Tsuei, L. H. Tjeng, *J. El. Spectr. Rel. Phenom. 198*, 6-11 (2015).

50. L. Misch, *Metallwirtsch. Metallwiss. Metalltech. 14*, 897-899 (1935).

51. K. Koepernik, H. Eschrig, *Phys. Rev. B*, *59*, 1743-1757 (1999).

52. V. Blum, R. Gehrke, F. Hanke, P. Havu, V. Havu, X. Ren, K. Reuter, M. Scheffler, *Comput. Phys. Commun. 180*, 2175-2196 (2009).

53. J. P. Perdew, Y. Wang, *Phys. Rev. B, 45*, 13244-13249 (1992).

54. M. B. Trzhaskovskaya, V. G. Yarzhemsky, *Atomic Data and Nuclear Data Tables*, *119*, 99-174, (2018).

55. M. Kohout, *Int. J. Quantum Chem.*, *97*, 651-658 (2004).

56. S. A. Villaseca, A. Ormeci, S. V. Levchenko, R. Schlögl, Yu. Grin, M. Armbrüster, *ChemPhysChem*, *18*, 334–337 (2017).

57. O. Madelung, Ed., *Semiconductors - Group IV Elements and II-V Compounds.* (Springer Berlin Heidelberg, 1991).

58. O. Madelung, Ed., *Semiconductors - Other than Group IV Elements and III -V Compounds*. (Springer Berlin Heidelberg, 1992).

59. W. M. Yim, *J. Appl. Phys. 40*, 2617-2623 (1969).

60. S. Öğüt. K. M. Rabe, *Phys. Rev. B, 51*, 10443-10453 (1995).

61. B. R. K. Nanda, I. Dasgupta, *J. Phys. Cond. Mat.* **15**, 7307-7323 (2003).

62. M. Imaia, T. Naka, T. Furubayashi, H. Abe *Appl. Phys. Lett.* **86**, 032102 (2005).

63. L. Siggelkow, V. Hlukhyy, T. F. Fässler, *J. Solid State Chem.* **191**, 76-89 (2012).

64. J. Evers, *J. Less-Comm. Met.* **58**, 75-83 (1978).

65. D. B. Migas, L. Miglio, V. L. Shaposhnikov, V. E. Borisenko,. *Phys. Rev. B*, **67**, 205203 (2003).

66. G. Cordier, H. Schäfer, M. Stelter, *Z. Naturforsch. B*, **39**, 727-732 (1984).

67. Q. Shi, Z. Feng, Y. Yan, Y. X. Wang, *RSC Adv.* **5**, 65133-65138 (2015).

68. Q. D. Gibson, H. Wu, T. Liang, M. N. Ali, N. P. Ong, Q. Huang, R. J. Cava, *Phys. Rev. B*, **91**, 085128 (2015).

69. H. Zhang, L. Fang, M.-B. Tang, H.-H. Chen, X.-X. Yang, X. Guo, J.-T. Zhao, Yu. Grin, *Intermetallics*, **18**, 193-198 (2010).

70. H. Mizoguchi, Y. Muraba, D. C. Fredrickson, S. Matsuishi, T. Kamiya, H. Hosono, *Angew. Chem. Int. Ed.* **56**, 10135-10139 (2017).

71. P. Koenig, D. W. Lynch, G. C. Danielson, *J. Phys. Chem. Solids*, **20**, 122-126 (1961).

72. R. D. Redin, R. G. Morris, G. C. Danielson, Semiconducting Properties of Mg_2Ge Single Crystals. *Phys. Rev.* **109**, 1916-1920 (1958).

73. H. G. Lipson. A. Kahan, *Phys. Rev.* **133**, A800--A810 (1964).

74. L. F. Mattheiss, *Phys. Rev. B*, **43**, 12549-12555 (1991).

75. D. Shinoda, S. Asanabe, Y. Sasaki, J. *Phys. Soc. Jap.* **19**, 269-272 (1964).

76. D. Mandrus, V. Keppens, B. C. Sales, and J. L. Sarrao. Phys. Rev. B 58, 3712 (1998)

77. J. Evers, G. Oehlinger, H. Meyer, *Mat. Res. Bull.* **19**, 1177-1180 (1984).

78. M. Springborg, R. Fischer, *J. Phys. Cond. Mat.* **10**, 701-716 (1998).

79. V. Yu. Verchenko, Z. Wei, A. A. Tsirlin, C. Callaert, A. Jesche, J. Hadermann, E. V. Dikarev, A. V. Shevelkov, *Chem. Mat.* **29**, 9954-9963 (2017).

80. W. Xie, L. Gustin, G. Bian. *Inorg. Chem.* **56**, 5165−5172 (2017).

81. M. Krajči, J. Hafner, *J. Phys. Cond. Mat.* **14**, 7201-7219 (2002).

82. U. Häussermann, M. Boström, P. Viklund, Ö. Rapp, T. Björnängen, *J. Solid State Chem.* **165**, 94-99 (2002).

83. Y. Amagai, A. Yamamoto, T. Iida, Y. Takanashi, *J. Appl. Phys.* **96**, 5644-5648 (2004).

84. D. Benson, O. F. Sankey, U. Häussermann, *Phys. Rev. B*, **84**, 125211 (2011).

85. D. M. Bercha, I. V. Slipukhina, M. Sznajder, K. Z. Rushchanskii, *Phys. Rev. B*, *70*, 235206 (2004).

86. Z. Schlesinger, Z. Fisk, H.-T. Zhang, M. B. Maple, J. DiTusa, G. Aeppli, *Phys. Rev. Lett. 71*, 1748-1751 (1993).

87. W. E. Spicer, A. H. Sommer, J. G. White. *Phys. Rev*. *115*, 57-62 (1959).

88. M. Aycibin, E. K. Dogan, S. E. Gulebaglan, M. N. Secuk, B. Erdinc, H. Akkus, *Comp. Cond. Mat. 1*, 32-37 (2014).

89. A. Karpov, J. Nuss, U. Wedig, M. Jansen, *Angew. Chem. Int. Ed*. *42*, 4818-4821 (2003).

90. N. E. Christensen, J. Kollar, *Solid State Comm. 46*, 727-730 (1983).